Determining the time-variable part of the toroidal geomagnetic field in the core-mantle boundary zone

J.M. Hagedoorn[a], H. Greiner-Mai[a], L. Ballani[a]

[a]*Helmholtz Center Potsdam, GFZ German Research Center for Geosciences, Section 1.5: Earth System Modelling, Telegrafenberg, D-14473 Potsdam, Germany*

Abstract

For the computation of the electromagnetic (EM) core-mantle coupling torque, the geomagnetic field must be known at the core-mantle boundary (CMB). It can be divided into linearly independent poloidal and toroidal parts. As shown by previous investigations, the toroidal field produces more than 90 % of the EM torque. It can be obtained by solving the associated (toroidal) induction equation for the electrically conducting part of the mantle, i.e. an initial boundary value problem (IBVP). The IBVP differs basically from that for the poloidal field by the boundary values at the interface between lower conducting and upper insulating parts of the mantle: the toroidal field vanishes, the poloidal field continues harmonically as potential field towards the Earth surface. The two major subjects are to find a suitable algorithm to solve the IBVP and to compute the toroidal geomagnetic field at the CMB. Compared to the poloidal field, the toroidal field at the CMB cannot be inferred from geomagnetic observations at the Earth's surface. In this study, it is inferred from the velocity field of the fluid core flow and the poloidal field at the CMB using an approximation which is consistent with the frozen-field approximation of the geomagnetic secular variation. This investigation differs from earlier ones by: (i) inferring the poloidal field at the CMB from the observed geomagnetic field using a rigorous inversion of the associated (poloidal) induction equation on which the fluid-flow inversion is based to determine consistently the surface flow velocities at the CMB, (ii) applying orthonormal spherical harmonic functions for the representation of the fields and torques, (iii) solving the IBVP numerically by a modified Crank-Nicolson algorithm, which (iv) allows us to highlight the influence of this approach on the resulting EM coupling torques. In addition to an outline of the derivations of the theoretical formalism and numerical methods, the time-variable toroidal field at the CMB is presented for different conductivity models.

Key words: toroidal geomagnetic field, induction process, core-mantle transition zone

1. Introduction

The toroidal geomagnetic field is bound to electrically conducting parts of the Earth and zero (not observable) outside. It plays a decisive role in dynamo theory, but also in electromagnetic core-mantle coupling. In this paper, we will present theoretical derivations and results obtained for the computation of the toroidal field within the framework of our study of EM core-mantle coupling, i.e. its determination as a prerequisite for the computation of EM torques, which are additionally presented here.

Different approaches were chosen to estimate the toroidal geomagnetic field in the Earth's mantle and/or core in the past. In some studies (e.g. Celaya and Benton, 1991; Love and Bloxham, 1994) EM coupling is used to relate the observed variations in length-of-day (LOD) to the necessary geomagnetic field in the Earth's mantle, assuming that EM coupling is the sole mechanism which causes LOD variations on decadal time scales. Beside this assumption, their approach is also limited to the steady fluid flows at the core-mantle boundary (CMB). This restrictive assumption and their problematic interpretation is discussed in Holme (1998a).

Other investigations are focused on the determination of the toroidal geomagnetic field in the core and consider also the CMB as a boundary with special conditions. For example, Levy and Pearce (1991) use measurements of the electrical potential in newly constructed submarine telegraph cables and use Green's functions to determine the boundary values at the CMB and the toroidal geomagnetic field in the core. Zhang and Fearn (1993) estimated the toroidal geomagnetic field based on stability investigations of the magneto-hydrodynamics of the outer core. A similar study was performed by Bhattacharyya (1995).

Our study follows the idea to set up proper boundary conditions at the CMB to determine the toroidal geomagnetic field. This idea was earlier published by Stix and Roberts (1984), but in contrast to our rigorous time-dependent formulation and solution they have introduced an iterative technique for the field determination.

In general, EM torques within the conducting regions of the Earth's mantle are produced by the Lorentz forces originated by the interaction of electric currents with the internal geomagnetic field. These currents are induced by temporal variations of the geomagnetic field in the mantle or leak from the core into the mantle. By using Ohm's law to express the current density, j, by the electric field, E, and eliminating the electric field in the Maxwell equations by the magnetic flux, B, we obtain a

differential equation of second order for $\boldsymbol{B}$, which is the so-called induction equation:

$$\frac{1}{\mu_0} \operatorname{curl}\left(\frac{1}{\sigma_{\mathrm{M}}} \operatorname{curl} \boldsymbol{B}\right) + \frac{\partial}{\partial t} \boldsymbol{B} = 0. \qquad (1)$$

In eq. (1), μ_0 is the permeability of vacuum. $\boldsymbol{B}$ fulfils the additional condition: div $\boldsymbol{B} = 0$. The induction equation is the basic equation describing how the geomagnetic field penetrates the conducting part of the mantle.

As shown by e.g. Jacobs (1987, Sec. 1.3.2), the vector $\boldsymbol{B}$ can be divided linearly independent into poloidal, $\boldsymbol{B}^{\mathrm{P}}$, and toroidal, $\boldsymbol{B}^{\mathrm{T}}$, parts: $\boldsymbol{B} = \boldsymbol{B}^{\mathrm{P}} + \boldsymbol{B}^{\mathrm{T}}$. For a radially dependent mantle conductivity, $\sigma_{\mathrm{M}}(r)$, the induction equation of the mantle can be divided adequately into independent induction equations for $\boldsymbol{B}^{\mathrm{P}}$ and $\boldsymbol{B}^{\mathrm{T}}$, respectively. The notation "poloidal" and "toroidal" introduced for vector fields has been extended to the EM torque (e.g. Stix and Roberts, 1984) to identify whether the associated part of the torque is produced solely by the poloidal field or by a combination of $\boldsymbol{B}^{\mathrm{P}}$ and $\boldsymbol{B}^{\mathrm{T}}$. It has been shown by several authors (e.g. Stix and Roberts, 1984; Greiner-Mai, 1993) that for physically reasonable values of σ_{M} the toroidal torque produces nearly the whole EM torque.

As shown by Rochester (1962), and recently by Hagedoorn and Geiner-Mai (2008), the EM torque can be represented by a surface integral over the CMB ($r = R_{\mathrm{CMB}}$), in which $\boldsymbol{B}$ is required. Therefore, the major problem of the torque computation is to infer the geomagnetic field at the CMB from its representations at the Earth's surface by the solution of the respective induction equation.

The associated initial-boundary value problems (IBVP) for $\boldsymbol{B}^{\mathrm{P}}$ and $\boldsymbol{B}^{\mathrm{T}}$ differ basically from each other. For $\boldsymbol{B}^{\mathrm{P}}$ the boundary value problem (BVP) is a one-side or side-ways ill-posed inverse BVP (according to the notation in inverse heat conduction theory, e.g. Ballani et al., 2002). For this case, the boundary values at the interface between the conducting lower and insulating upper mantle, $r = R_{\sigma}$ (see also Hagedoorn and Geiner-Mai, 2008, Fig. 3.1), can be inferred from the geomagnetic field at the Earth's surface, $r = R_{\mathrm{E}}$, by a harmonic downward continuation according to potential theory. The IBVP to determine $\boldsymbol{B}^{\mathrm{P}}$ in the corresponding electrical conducting part of the mantle is solved by the non-harmonic downward continuation (NHDC) developed by Ballani et al. (2002).

In contrast, the IBVP for $\boldsymbol{B}^{\mathrm{T}}$ is a two-side forward BVP, for which the boundary values are zero at R_{σ}, and those at R_{CMB} cannot be inferred directly from the observed geomagnetic field. In this second case, we calculate boundary values of the third kind by applying an additional boundary condition, derived from the continuity of the tangential component of $\boldsymbol{E}$. Thereby, we consider an approximation corresponding with the frozen-field theory (e.g. Backus, 1969) of the secular variation (SV) of the poloidal field (see Sec. 3.2). Based on this boundary values we solve rigorously the toroidal induction equation (Sec. 2 and 3.3) as an IBVP, to calculate the values of $\boldsymbol{B}^{\mathrm{T}}(R_{\mathrm{CMB}})$ on the mantle side, necessary for the determination of the coupling torques.

A precondition for the existence of currents and EM coupling torques on the mantle itself, is a non-zero mantle electrical conductivity. Most of the associated conductivity models are based on the assumption that regions with significant conductivity are concentrated in thin shells near the CMB, and are more or less reasoned by high pressure laboratory experiments (e.g. Dubrovinsky et al., 2003), nutation theory (e.g. Buffett, 1992) and investigations of EM torques (e.g. Holme, 1998b). A more detailed justification for the conductivity models chosen in our EM torque studies is given in a preliminary investigation of Greiner-Mai et al. (2007) (see also Sec. 4).

Our study is based on: (i) a rigorous inversion of the induction equation of the mantle, developed by Ballani et al. (2002) and Greiner-Mai et al. (2004) by which the poloidal geomagnetic field in the core-mantle boundary region can be inferred from the observed geomagnetic surface field; (ii) the reformulation of the orthonormal complex spherical harmonic (SH) functions according to Varshalovich et al. (1989), to obtain analytical expressions of EM torque components in dependence of the SH coefficients of the defining scalars of $\boldsymbol{B}^{\mathrm{P}}$ and $\boldsymbol{B}^{\mathrm{T}}$ (Sec. 2); (iii) development of a numerical method to solve the IBVP for $\boldsymbol{B}^{\mathrm{T}}$ which we will present here in Sec. 3.3. Compared with earlier investigations (e.g. Stix and Roberts, 1984; Greiner-Mai, 1987; Holme, 1998a) using quasi-stationary solutions, our solution is also rigorous with respect to the initial value problem. The formalism, the numerical implementation and corresponding derivations are described in Hagedoorn and Geiner-Mai (2008) so that we will refer to this monograph for more details. For the numerical calculation we use satellite supported geomagnetic field representations (Wardinski and Holme, 2006) with a high temporal resolution appropriate for the numerical method applied. We present results for toroidal fields at the CMB in Sec. 5 using preliminary conductivity models (see Sec. 4.2) and, for comparison, results from the perturbation approach used frequently (e.g. Stewart et al., 1995). Moreover, we show the related EM coupling torques based on the different approaches for the computation of the toroidal geomagnetic field at the CMB.

2. The induction equation of the toroidal field

The derivation of the induction equation (1) is only indicated, therefore, we summarize here the related equations. The fundamental equations for the derivation are the so-called pre-Maxwell equations (e. g. Backus, 1986),

$$\operatorname{curl} \boldsymbol{B} = \mu_0 \boldsymbol{j}, \qquad (2)$$

$$\operatorname{div} \boldsymbol{B} = 0, \qquad (3)$$

$$\operatorname{curl} \boldsymbol{E} = -\frac{\partial}{\partial t} \boldsymbol{B}, \qquad (4)$$

and Ohm's law

$$\boldsymbol{j} = \sigma \boldsymbol{E}. \qquad (5)$$

Here, we assume a radially dependent conductivity profile, $\sigma_{\mathrm{M}}(r)$, which leads considering Ohm's law and eqs. (2) and (4) to

$$\frac{1}{\mu_0} \operatorname{curl}\left(\frac{1}{\sigma_{\mathrm{M}}} \operatorname{curl} \boldsymbol{B}\right) + \frac{\partial}{\partial t} \boldsymbol{B} = 0. \qquad (6)$$

Furthermore, the geomagnetic field is divergence free (see eq. (3)) and can, therefore, be decomposed into its poloidal and toroidal parts by

$$\boldsymbol{B} = \boldsymbol{B}^{\text{P}} + \boldsymbol{B}^{\text{T}} = \text{curl curl}\,(\boldsymbol{r}\,S) + \text{curl}\,(\boldsymbol{r}\,T), \qquad (7)$$

where the functions S and T are the so-called field-generating scalars. These scalars are normalized in the way that their surface integral over the CMB vanishes (e.g. Krause and Rädler, 1980), which writes e. g. for T

$$\int_{\Omega} T\,\text{d}\Omega = 0, \qquad (8)$$

where $\text{d}\Omega$ denotes the spherical surface element.

Assuming an only radially varying conductivity profile, $\sigma_{\text{M}}(r)$, allows us to split the induction equation into independent poloidal and toroidal contributions. Using the definition in eq. (7) and some rules about the decomposition into poloidal and toroidal contributions, the toroidal part of the induction equation (6) is given by

$$\frac{1}{\mu_0}\,\text{curl}\left(\frac{1}{\sigma_{\text{M}}}\,\text{curl curl}\,(\boldsymbol{r}\,T)\right) + \frac{\partial}{\partial t}\,\text{curl}\,(\boldsymbol{r}\,T) = 0, \qquad (9)$$

which reads after some mathematical manipulations (see Appendix A.1)

$$\boldsymbol{r} \times \text{grad}\left[\frac{1}{\mu_0\sigma_{\text{M}}}\left(\Delta T - \frac{1}{r\sigma_{\text{M}}}\frac{\text{d}}{\text{d}r}\sigma_{\text{M}}\frac{\partial}{\partial r}(rT) - \frac{\partial}{\partial t}T\right)\right] = 0. \qquad (10)$$

The vector product shows a sole r-dependence of the expression (10) in the brackets. With the normalization of the field-generating scalar T in eq. (8), from which also follows $\int_{\Omega} \Delta T\,\text{d}\Omega = 0$, we can conclude

$$\int_{\Omega} \frac{1}{\mu_0\,\sigma_{\text{M}}}\left[\Delta T - \frac{1}{r\sigma_{\text{M}}}\frac{\text{d}}{\text{d}r}\sigma_{\text{M}}\frac{\partial}{\partial r}(rT) - \frac{\partial}{\partial t}T\right]\text{d}\Omega = 0. \qquad (11)$$

From $\boldsymbol{r} \times \text{grad}[f(r,\Omega)] = 0$, we can conclude in this line of arguments that $f(r,\Omega) = g(r)$ vanishes identically, i.e. eq. (10) is only satisfied if

$$\frac{1}{\mu_0\,\sigma_{\text{M}}}\left(\Delta T - \frac{1}{r\sigma_{\text{M}}}\frac{\text{d}}{\text{d}r}\sigma_{\text{M}}\frac{\partial}{\partial r}(rT) - \frac{\partial}{\partial t}T\right) = 0. \qquad (12)$$

The spherical harmonic (SH) representation of the field-generating scalar T is given by

$$T(r,\Omega) = \sum_{j=1}^{j_{\text{max}}} \sum_{m=-j}^{j} T_{jm}(r)Y_{jm}(\Omega), \qquad (13)$$

where the orthonormal spherical harmonic base functions, Y_{jm}, are defined according to Varshalovich et al. (1989, Chap. 5). The scalar induction equation (12) in SH representation can then be reduced to the following expression for each degree,

j, and order, m:

$$\frac{\partial^2}{\partial r^2}T_{jm}(r,t) + \left[\frac{2}{r} - \frac{1}{\sigma_{\text{M}}(r)}\frac{\partial}{\partial r}\sigma_{\text{M}}(r)\right]\frac{\partial}{\partial r}T_{jm}(r,t)$$

$$-\left[\frac{j(j+1)}{r^2} + \frac{1}{r\sigma_{\text{M}}(r)}\frac{\partial}{\partial r}\sigma_{\text{M}}(r)\right]T_{jm}(r,t) =$$

$$\mu_0\sigma_{\text{M}}(r)\frac{\partial}{\partial t}T_{jm}(r,t). \qquad (14)$$

More details of the derivation are given in Appendix A.1.

3. The initial boundary value problem for the toroidal field

In contrast to the BVP for the poloidal geomagnetic field, $\boldsymbol{B}^{\text{P}}$, no direct observed boundary values exist for the toroidal geomagnetic field, $\boldsymbol{B}^{\text{T}}$, because it vanishes outside of an electrical conductor. The necessary boundary value of T at the CMB must be inferred e. g. from known field quantities at the CMB. Here, we consider only that part of $\boldsymbol{B}^{\text{T}}$ which is produced by the interaction of the core motion with the poloidal field at the top of the core, giving the (small) variable part of the toroidal field. In this approach, we have to consider two restrictions: (i) we cannot quantify the toroidal "main field" and must, therefore, restrict to the time variable part of deduced quantities, and (ii) the resulting field is afflicted with the problem of ambiguity of the inversion of the frozen-flux equation by which the velocity field will be determined. The first restriction is not crucial, if we want to determine the EM coupling torques, because for such investigations only the variation of the torque and the observed Earth's rotation will be considered. In contrast, the second restriction affects our approach of EM coupling torque determination by the non-uniqueness of the necessary fluid-flow at the CMB, which is determined from the poloidal geomagnetic field and its time derivative at the CMB. This is discussed in Sec. 3.2 in more detail.

Primarily, we use the continuity of the tangential component of the electric field as boundary condition. From it, a boundary value for $\partial T/\partial r$ can only be inferred. $T(r = R_{\text{CMB}})$ itself must then be calculated by the solution of the related IBVP for which this additional boundary condition is used instead one for T itself.

3.1. Derivation of the boundary conditions for T

For any boundary at which the electrical conductivity changes, the magnetic flux $\boldsymbol{B}$ is continuous (e.g. Jacobs, 1987, Sec. 3.2.1). The poloidal and toroidal parts of the magnetic flux are linearly independent. Therefore, the continuity is valid for the toroidal part:

$$[\boldsymbol{B}^{\text{T}}]_-^+ = 0. \qquad (15)$$

The notation $[\ldots]_-^+$ denotes the difference between the related values infinitesimal above ($+$) and below ($-$) of the considered boundary. For the derivation of the boundary conditions for T, the relation between it and the toroidal flux, $\boldsymbol{B}^{\text{T}}$, in eq. (7) is used in eq. (15):

$$[-\boldsymbol{r} \times \text{grad}\,T]_-^+ = 0,$$

which leads to

$$-\boldsymbol{r} \times \operatorname{grad}(T^+ - T^-) = 0. \tag{16}$$

The expression in parentheses in eq. (16) is independent of ϑ and φ due to the vector product of $\boldsymbol{r}$ and the differential operator grad, which leads for a fixed r to a constant value:

$$(T^+ - T^-) = \text{const.}$$

Considering the integral normalization of T in eq. (8), we can conclude that the constant is zero, i.e.

$$T^+ = T^-.$$

Due to the orthonormal definition of the SH representation of T (see eq. (13)), the first boundary condition is

$$T_{jm}^+ = T_{jm}^-. \tag{17}$$

Beside the continuity of $\boldsymbol{B}^{\mathrm{T}}$, respectively T_{jm}, we have to introduce a second boundary condition at the CMB for the solving of the IBVP for T_{jm}. That is the continuity of the tangential component of the electrical field at the CMB (e.g. Greiner-Mai, 1986) which reads

$$\boldsymbol{r} \times (\boldsymbol{E}^+ - \boldsymbol{E}^-) = 0. \tag{18}$$

To relate this boundary condition for the electrical field to the field-generating scalar T, we express the electrical field above and below the CMB by $\boldsymbol{j}$ from eq. (5), and express $\boldsymbol{j}$ by $\boldsymbol{B}$ using eq. (2). In this way, we find for the electrical field above the CMB (in the mantle)

$$\boldsymbol{E}^+ = \frac{1}{\mu_0 \sigma_{\mathrm{M}}} \operatorname{curl} \boldsymbol{B}^+, \tag{19}$$

For the electrical field below the CMB, we have to consider additional contributions to the current density due to the relative velocity, $\boldsymbol{u}$, of the conducting liquid outer core material and, for a general description, an additional electrical field generated by possible turbulent flows, $\boldsymbol{E}^{\mathrm{F}}$:

$$\boldsymbol{j}^- = \sigma_{\mathrm{C}}(\boldsymbol{E}^- + \boldsymbol{u} \times \boldsymbol{B}^- + \boldsymbol{E}^{\mathrm{F}}), \tag{20}$$

where σ_{C} is the electrical conductivity in the fluid outer core. Hereby, we find for the electrical field below the CMB the expression

$$\boldsymbol{E}^- = \frac{1}{\mu_0 \sigma_{\mathrm{C}}} \operatorname{curl} \boldsymbol{B}^- - (\boldsymbol{u} \times \boldsymbol{B}^-) - \boldsymbol{E}^{\mathrm{F}}. \tag{21}$$

For the further derivation, we define analogously to eq. (7) field-generating scalars for the additional quantities in eq. (21). Here, we must consider that $\boldsymbol{u} \times \boldsymbol{B}$ is not divergence free and must be represented by three scalar functions. According to e. g. Krause and Rädler (1980, Sec. 13.4), the following decompositions

$$(\boldsymbol{u} \times \boldsymbol{B}^-)^{\mathrm{P}} = \boldsymbol{r} V + \operatorname{grad} W, \tag{22}$$

$$(\boldsymbol{u} \times \boldsymbol{B}^-)^{\mathrm{T}} = \operatorname{curl}(\boldsymbol{r} U), \tag{23}$$

$$\boldsymbol{E}^{\mathrm{FP}} = \boldsymbol{r} V^{\mathrm{F}} + \operatorname{grad} W^{\mathrm{F}}, \tag{24}$$

$$\boldsymbol{E}^{\mathrm{FT}} = \operatorname{curl}(\boldsymbol{r} U^{\mathrm{F}}), \tag{25}$$

are introduced and the related field-generating scalars U and V are normalized like T in eq. (8), that their surface integral over the CMB is identically zero.

The combination of the expressions (19)–(21) with the additional boundary condition in eq. (18) gives

$$\boldsymbol{r} \times \left[\frac{1}{\mu_0 \sigma_{\mathrm{M}}} \operatorname{curl} \operatorname{curl}(\boldsymbol{r} T^+) - \frac{1}{\mu_0 \sigma_{\mathrm{C}}} \operatorname{curl} \operatorname{curl}(\boldsymbol{r} T^-) \right.$$
$$\left. + \boldsymbol{r} V + \operatorname{grad} W + \boldsymbol{r} V^{\mathrm{F}} + \operatorname{grad} W^{\mathrm{F}} \right] = 0. \tag{26}$$

Applying the relation in eq. (51) from Appendix A.1 to curl curl($\boldsymbol{r} T$), we obtain

$$\boldsymbol{r} \times \operatorname{grad}\left(\frac{1}{\sigma_{\mathrm{M}}} \left[\frac{\partial}{\partial r}(rT) \right]^+ - \frac{1}{\sigma_{\mathrm{C}}} \left[\frac{\partial}{\partial r}(rT) \right]^- + \mu_0 W + \mu_0 W^{\mathrm{F}} \right) = 0. \tag{27}$$

To fulfill the condition in eq. (27) at the CMB ($r = R_{\mathrm{CMB}}$) the expression in the parentheses has to be constant. Due to the general representation of ($\boldsymbol{u} \times \boldsymbol{B}$) in eqs. (22)–(23), it is only possible to set up two normalization conditions for V and U. The field-generating scalars W and W^{F} are determined by ($\boldsymbol{u} \times \boldsymbol{B}$) except for arbitrary integration constants. It is possible to choose this additive constants, so that the following second boundary condition for T holds:

$$\frac{1}{\sigma_{\mathrm{C}}} \left[\frac{\partial}{\partial r}(rT) \right]^- - \frac{1}{\sigma_{\mathrm{M}}} \left[\frac{\partial}{\partial r}(rT) \right]^+ = \mu_0(W + W^{\mathrm{F}}). \tag{28}$$

We introduce further approximations to reduce the boundary condition and derive a boundary value of the third kind for T. First, we assume that W^{F} is identically zero, which means we neglect the contribution due to the turbulent flow, which are normally of small scales. This corresponds with the restriction of our investigation on decadal time scales. Moreover, we assume that

$$\frac{\sigma_{\mathrm{M}}}{\sigma_{\mathrm{C}}} \left[\frac{\partial}{\partial r}(rT) \right]^- \cong F$$

is temporally constant, which leads to

$$\left[\frac{\partial}{\partial r}(rT) \right]^+ \cong -\mu_0 \sigma_{\mathrm{M}} W + F. \tag{29}$$

This simplification is based on the conception, that F is determined to a large extent by the toroidal geomagnetic dynamo field, which varies very slowly with time, where the variations on the decadal time scale considered here, do not contribute significantly to F. This assumption was also suggested by Jault and LeMouël (1991) and is analogous to the conventional separation of $\boldsymbol{B}^{\mathrm{P}}$ into a main and secular variation field, where the different sources of the geomagnetic field are related to the specific field (dynamo processes to the "main field", CMB surface flow to the secular variation field). Therefore, we neglect F for the further investigation. With these assumptions, we can only determine the time-variable part of T. A time-independent part

of T can not be determined by this approach, i.e. any leakage of the temporally constant toroidal field of the outer core has to remain unconsidered. As mentioned in Sec. 3, this assumption affects the resulting toroidal field but not the variation of the computed EM coupling torques.

Following this line of arguments, the second boundary condition for the field-generating scalar T in eq. (28) can be transformed into a boundary value of the third kind:

$$\left[\frac{\partial}{\partial r}(rT)\right]^+ = -\mu_0 \sigma_{\mathrm{M}} W. \tag{30}$$

Due to the orthogonality of the SH, we can also conclude that the following relation holds:

$$\left[\frac{\partial}{\partial r}(rT_{jm})\right]^+ = -\mu_0 \sigma_{\mathrm{M}} W_{jm}. \tag{31}$$

3.2. Calculation of the boundary values at R_σ and R_{CMB}

Two boundaries are specified for the IBVP for the field-generating scalar T, where the first is the CMB, which prescribes the boundary between the solid mantle and the fluid outer core at $r = R_{\mathrm{CMB}}$. The second boundary at $r = R_\sigma$ prescribes the boundary between the electrically conducting and insulating mantle (see also Sec. 4).

At $r = R_\sigma$ eq. (17) is valid. Moreover, the toroidal geomagnetic field is zero in any electrically insulating part of the mantle, which leads to

$$T_{jm}^- = T_{jm}^+ = 0 \qquad \text{at} \quad r = R_\sigma. \tag{32}$$

For the CMB ($r = R_{\mathrm{CMB}}$) eq. (17) is also valid, but it is not possible to determine T_{jm}^- inside the outer core directly from any observation. Therefore, we can only determine the boundary value of the third kind, given in eq. (31), by calculating W_{jm} from the poloidal geomagnetic field, $\boldsymbol{B}^{\mathrm{P}}$, and the fluid-flow velocity, $\boldsymbol{u}$, at the CMB. The field-generating scalar S, representing $\boldsymbol{B}^{\mathrm{P}}$ at the CMB, is obtained by non-harmonic downward continuation (NHDC) of a global geomagnetic field model like C^{3}FM (Wardinski and Holme, 2006) according to Ballani et al. (2002). This non-harmonically downward continued quantities are used afterwards for a fluid-flow inversion according to Wardinski (2005) to determine the surface flow velocity $\boldsymbol{u}$ of the outer core fluid close to the CMB. It is known, that such an inversion is non-unique and needs additional constraint for the flow velocity determination. As by Wardinski (2005), here is assumed tangential geostrophy for the resulting $\boldsymbol{u}$. We use the surface velocity as input data for the determination of the boundary value which is therefore affected by this non-uniqueness of the fluid-flow inversion. A comprehensive discussion of the related problems of non-uniqueness in relation to the toroidal field and EM coupling torque determination can be found in Holme (1998a).

From the general decomposition of $(\boldsymbol{u} \times \boldsymbol{B})$ in eqs. (22) and (23), it is straight-forward to derive the following relation for the angular part of the Laplace operator in spherical coordinates, Δ_Ω, applied on W (e.g. see Hagedoorn and Geiner-Mai, 2008, Appendix D3)

$$\Delta_\Omega W = \boldsymbol{r} \cdot \mathrm{curl}\left[\boldsymbol{r} \times (\boldsymbol{u} \times \boldsymbol{B})\right]. \tag{33}$$

The definition of Δ_Ω and the derivation of the SH representation of W is given in the Appendix A.2, which leads to

$$W_{jm} = \frac{-1}{j(j+1)} \int_\Omega \boldsymbol{r} \cdot \mathrm{curl}\left[\boldsymbol{r} \times (\boldsymbol{u} \times \boldsymbol{B})\right] Y_{jm}^*(\Omega)\,\mathrm{d}\Omega. \tag{34}$$

Here, Y_{jm}^* denotes the complex conjugate of the SH. For the further derivation, we simplify the integral kernel and introduce scalars P and Q, representing the velocity field $\boldsymbol{u}$ at the CMB (see eqs. (61)–(62) in Appendix A.2). Moreover, using the SH representation of the scalars S, P and Q analogue to eq. (13), it is possible to reduce analytically the integral to a summation of this SH coefficients and related coefficients, which can be expressed by Clebsch-Gordan coefficients. This derivation is summarized in Appendix A.2 and leads to

$$W_{jm} = \frac{-1}{j(j+1)} \sum_{klst} k(k+1) S_{kl}(t)[\mathbf{L}_{klst}^{jm} P_{st}(t) - \mathbf{K}_{klst}^{jm} Q_{st}(t)], \tag{35}$$

where the integral-representing coefficients (see also eqs. (65)–(66) in Appendix A.2) are given by

$$\mathbf{K}_{klst}^{jm} = \frac{1}{2}\left[k(k+1) - s(s+1) - j(j+1)\right]$$
$$\cdot \sqrt{\frac{(2k+1)(2s+1)}{4\pi(2j+1)}}\, \mathbf{C}_{k0s0}^{j0}\, \mathbf{C}_{klst}^{jm}, \tag{36}$$

$$\mathbf{L}_{klst}^{jm} = \frac{i}{2}\sqrt{(k+s+j+2)(k+s-j)}$$
$$\cdot \sqrt{(k-s+j+1)(-k+s+j+1)}$$
$$\cdot \sqrt{\frac{(2k+1)(2s+1)}{4\pi(2j+3)}}\, \mathbf{C}_{k0s0}^{(j+1)0}\, \mathbf{C}_{klst}^{jm}. \tag{37}$$

Here, $\mathbf{C}_{klst}^{jm}$, denote the Clebsch-Gordan coefficients according to their definition in Varshalovich et al. (1989, Chap. 8) and $\sum_{klst}$ is an abbreviation for the summation over the degrees k and s and the related orders l and t.

Based on the SH representations for the field-generating scalars S, P and Q at the CMB it is now possible to determine the boundary value of the third kind in eq. (31) by eqs. (35)–(37).

3.3. Solving the IBVP for the toroidal field

The previous Sections 2 and 3.2 present the governing differential equation and the related boundary values for the IBVP of the toroidal geomagnetic field at the CMB and its SH representation by T_{jm}. To obtain a compact form of the governing partial differential equation (14), we introduce the following abbreviations:

$$\Phi = \left[\frac{2}{r} - \frac{1}{\sigma_{\mathrm{M}}(r)}\frac{\partial}{\partial r}\sigma_{\mathrm{M}}(r)\right], \tag{38}$$

$$\Theta = \left[\frac{j(j+1)}{r^2} + \frac{1}{r\sigma_{\mathrm{M}}(r)}\frac{\partial}{\partial r}\sigma_{\mathrm{M}}(r)\right], \tag{39}$$

$$\Psi = \mu_0 \sigma_{\mathrm{M}}(r). \tag{40}$$

Moreover, we use a reduced notation for the partial derivatives and neglect all arguments of the field-generating scalar, according to:

$$\mathsf{T} = T_{jm}(r, t), \tag{41}$$

$$\mathsf{T}_{,r} = \frac{\partial}{\partial r} T_{jm}(r, t), \tag{42}$$

$$\mathsf{T}_{,rr} = \frac{\partial^2}{\partial r^2} T_{jm}(r, t), \tag{43}$$

$$\mathsf{T}_{,t} = \frac{\partial}{\partial t} T_{jm}(r, t). \tag{44}$$

The initial-boundary value problem (IBVP) for the field-generating scalar T in its SH representation for an electrically conducting mantle is set up by the differential equation

$$\mathsf{T}_{,rr} + \Phi\, \mathsf{T}_{,r} - \Theta\, \mathsf{T} - \Psi\, \mathsf{T}_{,t} = 0 \tag{45}$$

and the boundary conditions at $r = R_\sigma$

$$\mathsf{T}^+ = \mathsf{T}^- = 0, \tag{46}$$

and at $r = R_{\text{CMB}}$

$$\mathsf{T}^+ = \mathsf{T}^- \quad \text{and} \quad [(r\mathsf{T})_{,r}]^+ = -\mu_0 \sigma_{\text{M}} W_{jm}. \tag{47}$$

In addition, we need to prescribe an initial value for $T_{jm}(r, t = 0)$.

The basic idea for the solution of the IBVP is to express all derivatives in the describing differential equation by finite differences. This method can be numerically implemented quite straight forward. We follow the common approach of finite differences (e.g. Ciarlet and Lions, 1990, Chap. I.1) to solve the partial differential equation (45) with respect to the spatial variable r, and the time t. As initial value we have chosen the solution of the related quasi-stationary problem (solving eq. (45) without the time-derivative). A detailed description of the numerical implementation and the related derivation is given in Hagedoorn and Geiner-Mai (2008, Sec. 4).

4. Input data and electrical conductivity models

4.1. Preparation of input data

The observed poloidal geomagnetic field and its representation by time-dependent SH coefficients, S_{jm}, at the Earth's surface are the only given input data for the computation of the toroidal geomagnetic field at the CMB. We choose the representation C^{3}FM of the geomagnetic field at the Earth's surface (Wardinski and Holme, 2006). This field model covers the time interval of the calendar year 1980–2000 with monthly resolution and a spatial resolution up to SH degree $j_{\max} = 15$. For all calculations and visualizations, we restrict the results and the related computation to the maximum SH degree $j_{\max} = 8$. By this, we want to ensure that all variations in the observed geomagnetic field (i.e. in the boundary condition) are related to processes in the Earth's core and are not significantly influenced by crustal magnetization or other processes (e.g. Greiner-Mai et al., 2007).
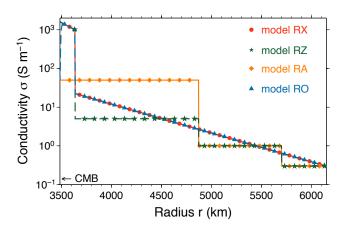

Figure 1: Electric conductivity model profiles RX ($2 \cdot 10^8$ S), RZ ($2 \cdot 10^8$ S), RA ($0.7 \cdot 10^8$ S) and RO ($1.9 \cdot 10^8$ S). The values in brackets are the conductance of the related model, i.e. the integral measure of the conductivity throughout the Earth's mantle.

In addition, we need for the determination of the toroidal geomagnetic field the field-generating scalar of the poloidal geomagnetic field (S) at the CMB and the generating scalars (P and Q) of the surface fluid-flow velocity, $\boldsymbol{u}$, in the outer core close to the CMB. We apply the NHDC considering one of the conductivity models (RX, RZ, RA and RO) presented in Sec. 4.2, to determine the poloidal geomagnetic field at the CMB. Wardinski (2005) has set up a fluid-flow inversion approach, where this time variable poloidal geomagnetic field is the main input. This method is applied here and we refer to the related publication as well as to Wardinski et al. (2008). The results discussed in Section 5 are based on those input data, where the fluid-flow inversion is based on the poloidal geomagnetic field at the CMB, determined by the NHDC.

4.2. Electrical conductivity models

For the determination of $\boldsymbol{B}^{\text{p}}$ and $\boldsymbol{u}$ presented above, we have to assume models for the stratification of the electrical conductivity in the Earth's mantle. In Fig. 1 are shown the four different applied conductivity models, which are motivated by different investigations. Recently, Otha et al. (2008) investigate the electrical conductivity of perovskite and post-perovskite under deep-mantle pressure and temperature conditions with laser-heated diamond-anvil cell experiments. They find an electrical conductivity of post-perovskite of more than $100\,\mathrm{S\,m^{-1}}$. In contrast, the measurements for perovskite are in the range between 0.01 and $1.0\,\mathrm{S\,m^{-1}}$. In addition, they emphasize that ~ 3 weight percent of $\mathrm{Al_2O_3}$ in the post-perovskite layer could increase the electrical conductivity by a factor of 3.5 (see also Xu et al., 1998a). The idea of a highly electrical conducting post-perovskite layer above the CMB is also published by Ono et al. (2006), based on shock-wave experiments on $\mathrm{Al_2O_3}$. In their conclusions, they come up with a model in which the spatial heterogeneous heat flow out of the core creates a heterogeneous conductivity distribution by a second phase transition from post-perovskite back to perovskite. The value of the electrical conductivity of post-perovskite in the so-called D''-
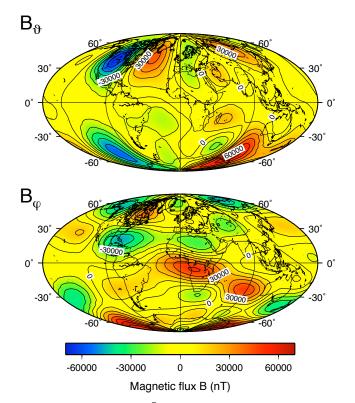
Figure 2: Both components of $\boldsymbol{B}^{\mathrm{T}}$ at the CMB for the calendar year 1993 considering the conductivity model RX (contour-lines for every 10000 nT).

Figure 3: Both components of $\boldsymbol{B}^{\mathrm{T}}$ at the CMB for the calendar year 1993 considering the conductivity model RZ (contour-lines for every 10000 nT).

layer above the CMB as well as the existence of the double-crossing of the phase transition between perovskite and post-perovskite is in debate in the last years (e.g. Ono et al., 2006; Xu et al., 1998b, 2000). Moreover, the influence of the electronic spin state is still in discussion (e.g. Bengtson et al., 2008; Lin et al., 2008; Stackhouse, 2008) and how the valence state (e.g. Zhang and Oganov, 2006) affects the electrical conductivity. Nagao et al. (2003) use observations of geomagnetic jerks to estimate the conductivity of the Earth's mantle, especially the differences of anomalies. Velímský et al. (2006) uses geomagnetic storms observed by the CHAMP satellite to invert for a one-dimensional conductivity profile. Their investigation confirms earlier findings that the electrical conductivity rises from $\sim 0.01\,\mathrm{S\,m^{-1}}$ in the upper mantle to $6\text{–}10\,\mathrm{S\,m^{-1}}$ in the upper part of the lower mantle (e.g. Olsen, 1998; Constable and Constable, 2004; Kuvshinov and Olsen, 2006). Buffett et al. (2002) constrain the electrical conductivity by the modelling of the nutation and precession of Earth's rotation including electromagnetic coupling. They conclude that a conductance (i.e. the integral measure of the conductivity throughout the mantle) of $\sim 10^8\,\mathrm{S}$ is necessary to explain the phase shifts in the observed nutation and precession.

Based on these different findings, we set up four different conductivity models. Model RX is a simplified representation of the high-pressure experiments with a highly conducting layer above the CMB. With model RZ, we consider in addition the results of the EM induction studies mentioned above. As an alternative to model RZ, we introduce model RA, which considers that EM induction studies do not resolve the lowermost
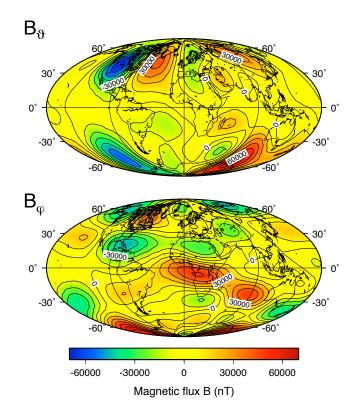
mantle. Moreover, with model RO we take into account that a double-crossing of the phase boundary between perovskite and post-perovskite is possible close to the CMB (e.g. Ono et al., 2006)

5. Discussion of numerical results

In Sec. 3, we have summarized the applied method to compute the toroidal geomagnetic field at the CMB based on the field-generating scalars S, P and Q inferred from geomagnetic observations. For the time series of the input data (1980–2000), we calculate the toroidal field by a Crank-Nicolson approach, which uses a LU-decomposition with partial pivoting, performed once at the beginning, and the related back substitution for each time step (e.g. Press et al., 1992, Sec. 2.3).

Figs. 2–5 show the ϑ- and φ-component of the toroidal geomagnetic field (B_r is sole poloidal) at the CMB considering the different conductivity models, each for the begin of the calendar year 1993 as an example. The extrema are in the order of ± 60000 nT for the conductivity models RX (Fig. 2) and RZ (Fig. 3), which is only around 12 % of the poloidal field strength (e.g. Hagedoorn and Geiner-Mai, 2008). Here, we emphasize that using the condition (31) we only determine the time-variable part of the toroidal field (see Sec. 3.1), whereas the poloidal field also contains the (quasi-) stationary dynamo field as "main field". Studies like those of Celaya and Benton (1991); Love and Bloxham (1994), found toroidal geomagnetic field strengths at the CMB in the order of 10^6 nT. Those estimations of the toroidal fields are based on the observed variation in
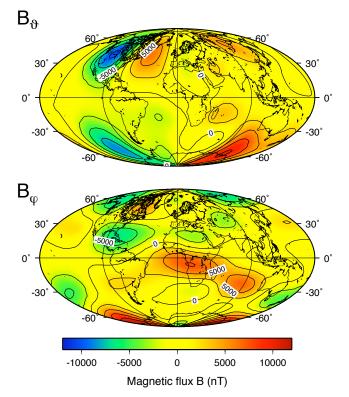
7

Figure 4: Both components of $\boldsymbol{B}^{\mathrm{T}}$ at the CMB for the calendar year 1993 considering the conductivity model RA (contour-lines for every 2500 nT).

Figure 5: Both components of $\boldsymbol{B}^{\mathrm{T}}$ at the CMB for the calendar year 1993 considering the conductivity model RO (contour-lines for every 5000 nT) .

LOD and the assumption that the responsible core-mantle coupling is solely an EM coupling. Moreover, Love and Bloxham (1994) restricted their investigation to steady fluid flows at the CMB. Those do not produce predominantly the variation of the EM coupling torque, these are the time-varying flow and the geomagnetic field.

In the results for the conductivity models RA (Fig. 4) and RO (Fig. 5), the extrema are only in the order of ± 10000 nT and ± 20000 nT, respectively. Common features in the ϑ-component are the dipolar structure in the northern hemisphere, which is located along $270°$ E with the extrema around $45°$ N. A much weaker dipolar structure can be found on the northern hemisphere, which spread out from $0° - 180°$ E. The most prominent feature in the southern hemisphere of the ϑ-component is a large-size structure with a maximum along $135°$ E and a minimum along $225°$ E. Those structures remain throughout the whole time series. Most conspicuous spatial pattern for the φ-component of the toroidal geomagnetic field, which is visible in all results, is an elongated structure along the equator with an minimum in the northern and a maximum in the southern hemisphere.

As for all other spatial patterns, which are detectable in all results, the amplitudes are significantly dependent on the conductivity model. For the conductivity models RX and RZ, similar toroidal geomagnetic fields are obtained. If the conductance is varied from $2 \cdot 10^8$ S for RX and RZ to $0.7 \cdot 10^8$ S for RA, than the amplitudes of the dominant spatial pattern reduce by a factor of 6.

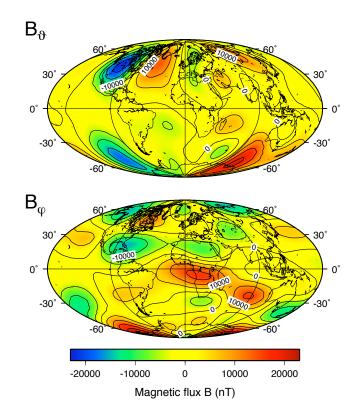A different result can be observed for the conductivity model

RO, which has a conductance of $\sim 1.9 \cdot 10^8$ S but in contrast to the other models a value of 50 S m^{-1} at the CMB. In this case the resulting extrema are reduced by a factor of 3. This observations lead to the conclusion, that the radial stratification can have a significant influence on the toroidal geomagnetic field at the CMB, where the spatial pattern are significantly determined by the spatial patterns of the poloidal geomagnetic and fluid-flow velocity fields at the CMB. A so-called perturbation method (e.g. Stewart et al., 1995; Holme, 1998a) for the downward continuation and the computation of the toroidal geomagnetic field would not be able to consider such differences as between the models RX and RO, because the conductivity stratification is considered by an integral value.

For a comparison with the perturbation method (e.g. Benton and Whaler, 1983), we choose therefore a more suitable conductivity model; a 2 km thick layer above the CMB with a constant conductivity of 10000 S m^{-1} (labeled P3). We use the formalism of Ballani et al. (2002, eqs. (42)–(43)) to implement the perturbation solution of the poloidal geomagnetic field. In addition, the authors compare therein the results for the perturbation method and the NHDC. For the determination of the toroidal field, we follow for the approach of Stewart et al. (1995). For both solution methods the poloidal geomagnetic field is determined at the CMB and used as input for the fluid-flow inversion. For the computation of the toroidal geomagnetic field at the CMB, the particular poloidal geomagnetic and fluid-flow velocity fields are considered.

In Fig. 6 are shown the differences in the resulting toroidal field components at the CMB for the year 1993. The maximal
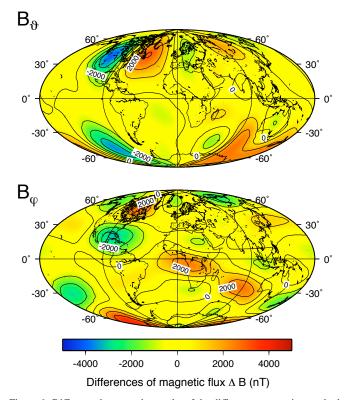
B_ϑ

B_φ

Differences of magnetic flux ΔB (nT)

Figure 6: Difference between the results of the different computation methods (rigorous IBVP, perturbation method) for both components of $\boldsymbol{B}^{\mathrm{T}}$ at the CMB. The differences are shown for the calendar year 1993 considering the conductivity model P3 (contour-lines for every 1000 nT).
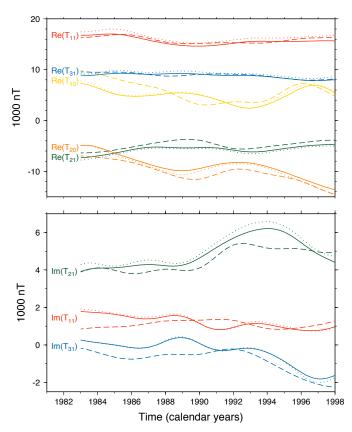

Figure 7: Real and imaginary part of the toroidal SH coefficients, $T_{jm}(r)$, at the CMB for different solution methods and input models. We compare results from the rigorous solution of the IBVP (solid line) with those from the perturbation approach (dotted lines) and for the perturbation approach and only harmonically downward continued input data (dashed line).

differences are in the order of ±3000 nT, which is about 5 % of the toroidal field. The spatial pattern is similar to that of the toroidal field itself (not shown here, but comparable with results of RX in Fig. 2). The amplitudes of the differences are strongly time-dependent. Hence, we compare in Figs. 7–8 the time behavior of the real and imaginary part for selected SH coefficients $T_{jm}(t)$, as defined in eq. (13) for the different methods. We show the results for: (i) the perturbation method (dotted lines), (ii) the rigorous solution of the IBVP (solid lines), and (iii) for the perturbation method applied for the determination of the toroidal field, but using only the harmonically downward continued poloidal field and the related fluid-flow velocities (dashed lines). Some of the resulting SH coefficients for (iii) differ from the related results for the rigorous solution by more than 100 %, but those differences are strongly time dependent (e.g. $\mathrm{Re}(T_{40})$, $\mathrm{Im}(T_{42})$, etc.). This should highlight the necessity to consider a non-harmonic downward continuation or perturbation method for the poloidal geomagnetic field and the related fluid-flow inversion.

The remaining differences between the rigorous solution of the IBVP for the toroidal field (solid line) and a perturbation method (dotted line) can still reach up to 5 % in most SH coefficients. This is related to the solution of the IBVP, which considers the time evolution and the diffusion rigorously. The occurrence of significant differences is dependent of SH degree and order. In some coefficients, like $\mathrm{Re}(T_{11})$ and $\mathrm{Re}(T_{42})$, a nearly constant overestimation can be observed, and in other co-

efficients ($\mathrm{Re}(T_{20})$, $\mathrm{Re}(T_{40})$, $\mathrm{Im}(T_{42})$ etc.) the differences vary strongly with time.

As mentioned in the introduction, one of the main motivations for a rigorous solution of the IBVP for the toroidal geomagnetic field is its necessity for the determination of the electromagnetic (EM) core-mantle coupling torque (e.g. Rochester, 1960; Roberts, 1972; Stix and Roberts, 1984; Greiner-Mai, 1993; Holme, 1998a). For this reason, we present in Fig. 9 a comparison of the variation of the EM coupling torques (the applied formalism is published by Hagedoorn and Geiner-Mai, 2008) using the different conductivity models. In addition, we also show the results based on the perturbation method explained above. In all three components (where ΔL_x and ΔL_y are related to the polar motion and ΔL_z to the variation in length-of-day) similar time behavior for the different results can be observed, whereas the amplitude differs up to a factor of nearly 10.

The different amplitudes are not only a result of different conductance of the conductivity models, as it can be seen by a comparison of the torques for the models RX and RO (like for the toroidal geomagnetic field), which differ only slightly in their conductance but significantly in their values of the conductivity at the CMB (1600 S m^{-1} vs. 50 S m^{-1} respectively). The models RX and RZ have the same conductance. Therefore, the

9
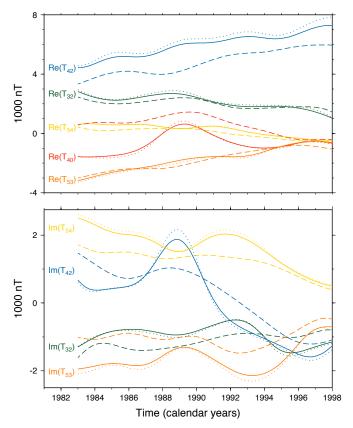
Figure 8: Same as Fig. 7 for additional SH coefficients.

Figure 9: Comparison of the variation of the electromagnetic coupling torque for the considered conductivity models (RX, RZ, RA and RO) and different solution techniques (rigorous solution: P3, perturbation solution AP3).
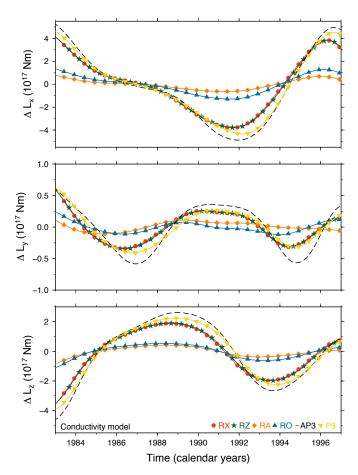
differences in the associated torques are caused by differences in the radial stratification of the conductivity. The influence of the reduced thickness of a conducting layer with the same conductance is visible in the differences between the torques for the models RX and P3; the amplitudes in all components are comparable but a time shift is clearly visible. Using the geomagnetic fields and the fluid-flow velocities determined by the perturbation method leads to a systematic overestimation of the amplitudes of the coupling torques up to 20 % for the x- and z-component and even up to 50 % for the y-component. In addition, we can detect a time shift relative to the results for P3 as well as for the whole mantle conductivity models.

6. Conclusions

Our investigation can be seen as a continuation in the development of rigorous methods of the determination of the geomagnetic field in the CMB region, which has begun several years ago by Ballani et al. (2002) and is embedded in the development of the description of the core-mantle interactions. In this article, we developed a theoretical description of the IBVP for the toroidal geomagnetic field in an electrical conducting mantle. Special assumptions about the generation of the toroidal field at the top of the CMB allows us only to determine the time-variable part of the toroidal field in the electrically conducting mantle (Sec. 3.1). By these assumptions, the resulting toroidal field is affected by the ambiguity of the fluid-flow velocities at the CMB, which are determined under the

frozen-flux approximation (for detailed discussion see Holme, 1998a). Beside the formulation of a Crank-Nicolson schema for the numerical implementation, we derived analytical solutions of coupling integrals between the surface-flow velocity and the poloidal geomagnetic field at the CMB to calculate boundary values of the third kind (given in eq. (31)). Numerical calculations were performed to determine the time-variable toroidal geomagnetic field at the CMB based on satellite supported poloidal geomagnetic field models and assumed conductivity models. In addition, we show a comparison of the resulting EM coupling torque variation for the time series of the geomagnetic field model.

The choice of our conductivity models is motivated by the EM coupling torque computation. Recent investigation of the electrical conductivity, summarized in Sec. 4, only constrain the lower and upper bounds of the conductivity for different depths, which is reflected in the chosen simplified conductivity models. In addition to the theoretical description of the determination of the time-variable toroidal geomagnetic field at the CMB, our first numerical results show a significant influence of the conductivity models by their value at the CMB and their integral measure (conductance) as shown in the comparison of results for the conductivity models RX, RA and RO.

For the comparison with the perturbation method, we consider a suitable thin-layer conductivity model (P3), which consists only of one 2 km thick highly conducting layer with constant $\sigma_M = 10000\,\mathrm{S\,m^{-1}}$. The comparison of the resulting toroidal geomagnetic field at the CMB for the two approaches shows similar spatial patterns, which differ by around 5 %. Those differences are strongly time-dependent, which is visible in the SH coefficients (see Figs. 7–8) and also reach 5 %. This findings lead us to the conclusion that the rigorous solution of the IBVP for the geomagnetic field in connection with the NHDC for the determination of the poloidal geomagnetic field at the CMB has a significant influence on the time-behavior of the resulting field.

This influence is also visible in the comparison of the related EM coupling torques for the different solution approaches, where the differences in the geomagnetic field leads to an time shift and a systematic overestimation of the torques based on the results of the perturbation method relative to our approach.

A. Appendix

A.1. Additional derivations for the toroidal geomagnetic field

In Sec. 2, the derivation of eq. (10) starting from eq. (9) is suppressed for readability and is summarized here. Considering the r-dependence of σ_M and the following relations for the differential operator curl, and any vector $\mathbf{v}$ and any scalar s (e.g. Bronstein et al., 1997, Sec. 13.2.5),

$$\mathrm{curl}\,(s\mathbf{v}) = s\,\mathrm{curl}\,\mathbf{v} + \mathrm{grad}\,s \times \mathbf{v}, \qquad (48)$$

$$\mathrm{curl}\,(\mathbf{v}_1 + \mathbf{v}_2) = \mathrm{curl}\,\mathbf{v}_1 + \mathrm{curl}\,\mathbf{v}_2, \qquad (49)$$

the toroidal induction equation reads:

$$\frac{1}{\mu_0}\left[\frac{1}{\sigma_M}\,\mathrm{curl}\,\mathrm{curl}\,\mathrm{curl}\,(\mathbf{r}T) + \mathrm{grad}\,\frac{1}{\sigma_M} \times \mathrm{curl}\,\mathrm{curl}\,(\mathbf{r}T)\right]$$
$$+ \frac{\partial}{\partial t}\,\mathrm{curl}\,(\mathbf{r}T) = 0. \qquad (50)$$

Furthermore, we consider the relations (e. g. Krause and Rädler, 1980, Sec. 13.3)

$$\mathrm{curl}\,\mathrm{curl}\,(\mathbf{r}T) = -\mathbf{r}\Delta T + \mathrm{grad}\left(\frac{\partial}{\partial r}rT\right), \qquad (51)$$

$$\mathrm{curl}\,\mathrm{curl}\,\mathrm{curl}\,(\mathbf{r}T) = \mathbf{r} \times \mathrm{grad}\,(\Delta T), \qquad (52)$$

which leads to the following toroidal induction equation:

$$\frac{1}{\mu_0\sigma_C}[\mathbf{r} \times \mathrm{grad}\,(\Delta T)]$$
$$+ \frac{1}{\mu_0}\left[\mathrm{grad}\,\frac{1}{\sigma_M} \times \left(-\mathbf{r}\Delta T + \mathrm{grad}\left(\frac{\partial}{\partial r}rT\right)\right)\right]$$
$$- \frac{\partial}{\partial t}(\mathbf{r} \times \mathrm{grad}\,T) = 0. \qquad (53)$$

For the further derivation, we have to reformulate the second term in the equation above, which reads with $\mathbf{r} = r\mathbf{e}_r$, a spherical symmetric conductivity σ_M and its related partial derivative $\mathbf{e}_r \frac{\mathrm{d}}{\mathrm{d}r}\frac{1}{\sigma_M} = -\mathbf{r}\frac{1}{r\sigma_M^2}\frac{\mathrm{d}}{\mathrm{d}r}\sigma_M$:

$$\frac{1}{\mu_0}\left[\left(\mathbf{r}\frac{1}{r\sigma_M^2}\frac{\mathrm{d}}{\mathrm{d}r}\sigma_M \times \mathbf{r}\Delta T\right) - \left(\mathbf{r}\frac{1}{r\sigma_M^2}\frac{\mathrm{d}}{\mathrm{d}r}\sigma_M \times \mathrm{grad}\left(\frac{\partial}{\partial r}rT\right)\right)\right] =$$
$$\frac{1}{\mu_0\,\sigma_M}\left[-\mathbf{r} \times \mathrm{grad}\left(\frac{1}{r\sigma_M}\frac{\mathrm{d}}{\mathrm{d}r}\sigma_M\frac{\partial}{\partial r}rT\right)\right]. \qquad (54)$$

We also consider that due to the sole r-dependence of the conductivity the following relation is valid:

$$\mathbf{r}\frac{1}{r\sigma_M}\frac{\mathrm{d}}{\mathrm{d}r}\sigma_M \times \mathrm{grad}\left(\frac{\partial}{\partial r}rT\right) = \mathbf{r} \times \mathrm{grad}\left(\frac{1}{r\sigma_M}\frac{\mathrm{d}}{\mathrm{d}r}\sigma_M\frac{\partial}{\partial r}rT\right).$$

First, we exchange the second term in eq. (53) by eq. (54) and, secondly, we consider that the following is valid for any scalar function a and b:

$$\mathbf{r} \times \mathrm{grad}\,a + \mathbf{r} \times \mathrm{grad}\,b = \mathbf{r} \times \mathrm{grad}\,(a + b).$$

This leads for the toroidal induction equation to:

$$\mathbf{r} \times \mathrm{grad}\left[\frac{1}{\mu_0\sigma_M}\left(\Delta T - \frac{1}{r\sigma_M}\frac{\mathrm{d}}{\mathrm{d}r}\sigma_M\frac{\partial}{\partial r}(rT) - \frac{\partial}{\partial t}T\right)\right] = 0,$$

which is identical with eq. (10).

Moreover, in Sec. 2 is given in eq. (14) the SH representation of the toroidal induction equation. In the following, the derivation starting from eq. (10) is summarized. Applying the SH representation of the field-generating scalar in eq. (13) and introducing the symbol $\sum_{jm}$ for the summation of j and m on the toroidal induction equation leads to

$$\sum_{jm}\left\{\frac{1}{\mu_0\sigma_M(r)}\left[\Delta T_{jm}(r,t)Y_{jm}(\Omega)\right.\right.$$
$$\left.- \frac{1}{r\sigma_M(r)}\frac{\mathrm{d}}{\mathrm{d}r}\sigma_M(r)\frac{\partial}{\partial r}(rT_{jm}(r,t))Y_{jm}(\Omega)\right]$$
$$\left.- \frac{\partial}{\partial t}T_{jm}(r,t)Y_{jm}(\Omega)\right\} = 0. \qquad (55)$$

We split now the Laplace operator into its radial and angular part (eq. (58)), and apply the angular part on the SH base function in eq. (59) (e.g. Varshalovich et al., 1989, Chap. 5), which leads to

$$\sum_{jm} \left\{ \frac{1}{\mu_0 \sigma_{\mathrm{M}}(r)} \left[\frac{1}{r^2} \left(\frac{\partial}{\partial r} (r^2 \frac{\partial}{\partial r} T_{jm}(r,t)) \right. \right. \right.$$

$$\left. - j(j+1) T_{jm}(r,t) \right)$$

$$\left. - \frac{1}{r \sigma_{\mathrm{M}}(r)} \frac{\mathrm{d}}{\mathrm{d}r} \sigma_{\mathrm{M}}(r) \frac{\partial}{\partial r} (r T_{jm}(r,t)) \right]$$

$$\left. - \frac{\partial}{\partial t} T_{jm}(r,t) \right\} Y_{jm}(\Omega) = 0. \tag{56}$$

Due to the orthogonality of the SH, we can conclude that each equation for any j and m has to be satisfied. Implementing the radial derivatives, we can find the equation:

$$\frac{1}{\mu_0 \sigma_{\mathrm{M}}(r)} \left[\frac{2}{r} \frac{\partial}{\partial r} T_{jm}(r,t) + \frac{\partial^2}{\partial r^2} T_{jm}(r,t) \right.$$

$$- \frac{j(j+1)}{r^2} T_{jm}(r,t)$$

$$\left. - \frac{1}{\sigma_{\mathrm{M}}(r)} \frac{\mathrm{d}}{\mathrm{d}r} \sigma_{\mathrm{M}}(r) \left(T_{jm}(r,t) + r \frac{\partial}{\partial r} T_{jm}(r,t) \right) \right]$$

$$- \frac{\partial}{\partial t} T_{jm}(r,t) = 0, \tag{57}$$

where a reordering with respect to the order of the partial derivatives of the coefficients T_{jm} leads to eq. (14).

A.2. Additional derivations for the boundary value

In Sec. 3.2, we introduce the angular part of the Laplace operator in spherical coordinates, which is given by

$$\Delta_{\Omega} = \left[\frac{1}{\sin \vartheta} \frac{\partial}{\partial \vartheta} \left(\sin \vartheta \frac{\partial}{\partial \vartheta} \right) + \frac{1}{\sin^2 \vartheta} \frac{\partial}{\partial \varphi^2} \right]. \tag{58}$$

The SH are eigenfunctions of the angular part of the Laplace operator so that

$$\Delta_{\Omega} Y_{jm}(\Omega) = -j(j+1) Y_{jm}(\Omega) \tag{59}$$

is valid. For the derivation of eq. (34), we apply the angular Laplace operator on the SH representation of W, according to eq. (59),

$$\Delta_{\Omega} W(r, \Omega, t) = \sum_{jm} W_{jm}(r,t) \Delta_{\Omega} Y_{jm}(\Omega),$$

$$= -\sum_{jm} j(j+1) W_{jm}(r,t) Y_{jm}(\Omega).$$

Next, we substitute $\Delta_{\Omega} W$ by eq. (33) and divide this equation by $-j(j+1)$ and multiply it with $Y_{jm}^*(\Omega)$. Considering the orthogonality of the SH leads then to

$$W_{jm} = \frac{-1}{j(j+1)} \int_{\Omega} \boldsymbol{r} \cdot \mathrm{curl} \left[\boldsymbol{r} \times (\boldsymbol{u} \times \boldsymbol{B}) \right] Y_{jm}^*(\Omega) \, \mathrm{d}\Omega,$$

which is identically with eq. (34).

For the derivation of eq. (35) in Sec. 3.2 starting from the integral expression (34), we simplify first the integral kernel in spherical coordinates, considering that $u_r = 0$ at $r = R_{\mathrm{CMB}}$,

$$\boldsymbol{r} \cdot \mathrm{curl} \left[\boldsymbol{r} \times (\boldsymbol{u} \times \boldsymbol{B}) \right] = \boldsymbol{r} \cdot \mathrm{curl} \left(\boldsymbol{u} \, r \, B_r \right),$$

which explicitly reads

$$\left[\boldsymbol{r} \cdot \mathrm{curl} \left(\boldsymbol{u} \, r \, B_r \right) \right]_r = \frac{r}{r \sin \vartheta} \left[\frac{\partial}{\partial \vartheta} (r B_r u_\varphi \sin \vartheta) - \frac{\partial}{\partial \varphi} (r B_r u_\vartheta) \right]. \tag{60}$$

For the vector components of the velocity field $\boldsymbol{u}$, we define the following decomposition with the representing scalars P and Q

$$u_\vartheta = \frac{\partial}{\partial \vartheta} P + \frac{1}{\sin \vartheta} \frac{\partial}{\partial \varphi} Q, \tag{61}$$

$$u_\varphi = \frac{1}{\sin \vartheta} \frac{\partial}{\partial \varphi} P - \frac{\partial}{\partial \vartheta} Q. \tag{62}$$

With the definition of the angular Laplace operator in eq. (58) and the decomposition of the magnetic flux in eq. (7), it can be shown that

$$B_r = -\frac{1}{r} \Delta_{\Omega} S. \tag{63}$$

Applying the expressions (60)–(63) to eq. (34), we find

$$W_{jm} = \frac{-1}{j(j+1)} \int_{\Omega} \frac{1}{\sin \vartheta} \left\{ \frac{\partial}{\partial \vartheta} \left[-\Delta_{\Omega} S \left(\frac{\partial}{\partial \varphi} P - \sin \vartheta \frac{\partial}{\partial \vartheta} Q \right) \right] \right.$$

$$\left. - \frac{\partial}{\partial \varphi} \left[-\Delta_{\Omega} S \left(\frac{\partial}{\partial \vartheta} P + \frac{1}{\sin \vartheta} \frac{\partial}{\partial \varphi} Q \right) \right] \right\} Y_{jm}^*(\Omega) \, \mathrm{d}\Omega. \tag{64}$$

For the next step, all field-generating scalars (S, P and Q) are represented by SH analogue to eq. (13) for the field-generating scalar T. After applying the product rule for the partial derivatives and the angular part of the Laplace operator, additional rearranging and combining of the partial derivatives (see Hagedoorn and Geiner-Mai, 2008, Appendix D.3) lead to the expression

$$W_{jm} = \frac{-1}{j(j+1)} \sum_{klst} k(k+1) S_{kl} [\mathbf{L}_{klst}^{jm} P_{st} - \mathbf{K}_{klst}^{jm} Q_{st}],$$

where

$$\sum_{klst} = \sum_{k=1}^{k_{\max}} \sum_{l=-k}^{k} \sum_{s=1}^{s_{\max}} \sum_{t=-s}^{s},$$

$$\mathbf{K}_{klst}^{jm} = \int_{\Omega} \left[\frac{\partial}{\partial \vartheta} Y_{kl}(\Omega) \frac{\partial}{\partial \vartheta} Y_{st}(\Omega) \right.$$

$$+ \frac{1}{\sin^2 \vartheta} \frac{\partial}{\partial \varphi} Y_{kl}(\Omega) \frac{\partial}{\partial \varphi} Y_{st}(\Omega)$$

$$\left. + Y_{kl}(\Omega) \Delta_{\Omega} Y_{st}(\Omega) \right] Y_{jm}^*(\Omega) \, \mathrm{d}\Omega, \tag{65}$$

$$\mathbf{L}_{klst}^{jm} = \int_{\Omega} \frac{1}{\sin \vartheta} \left[\frac{\partial}{\partial \vartheta} Y_{kl}(\Omega) \frac{\partial}{\partial \varphi} Y_{st}(\Omega) \right.$$

$$\left. - \frac{\partial}{\partial \varphi} Y_{kl}(\Omega) \frac{\partial}{\partial \vartheta} Y_{st}(\Omega) \right] Y_{jm}^*(\Omega) \, \mathrm{d}\Omega. \tag{66}$$

It remains to solve analytically both integrals above to derive the integral-representing coefficients (36) and (37) in Sec. 3.2 in terms of Clebsch-Gorden coefficients. The triple product of SH with different degrees and orders in eq. (65) is expressible by a combination of re-normed Clebsch-Gorden coefficients (Varshalovich et al., 1989, Sec. 5.9.1, eq. 4). Moreover, for the mixed partial derivatives in eq. (65) is given a relation to Clebsch-Gorden coefficients in Pěč and Martinec (1988, eq. 11). The derivation of $\mathbf{L}_{klst}^{jm}$ is more extensive, because the mixed partial derivatives of SH multiplied by $\frac{1}{\sin\vartheta}$ in eq. (66) can be expressed by the radial component of the vector product of vector spherical harmonics ($\boldsymbol{e}_r \cdot [\boldsymbol{S}_{kl}^{(0)}(\Omega) \times \boldsymbol{S}_{st}^{(0)}(\Omega)]$). The integral is expressed by Clebsch-Gorden coefficients considering different relation between vector and scalar spherical harmonics by so-called Wigner $9j$ symbols and related expressions according to Varshalovich et al. (1989, Chap. 7 & 8). The extensive mathematical manipulations of the detailed derivation are skipped here and can be found in Hagedoorn and Geiner-Mai (2008, Appendix D.4–D.5).

References

Backus, G., 1969. Kinematics of the geomagnetic secular variation in a perfectly conducting core. Phil. Trnas. R. Soc. London A, 263, 239–266.

Backus, G., 1986. Poloidal and toroidal fields in geomagnetic field modeling. Rev. Geophys. 24, 75–109.

Ballani, L., Greiner-Mai, H., Stromeyer, D., 2002. Determining the magnetic field in the core-mantle boundary zone by non-harmonic downward continuation. Geophys. J. Int. 149, 374–389.

Bengtson, A., Persson, K., Morgan, D., 2008. Ab inition study of the composition dependence of the pressure-induced spin crossover in persovskite $(Mg_{1-x},Fe_x)SiO_3$. Earth Planet. Sci. Lett. 265, 535–545.

Benton, E., Whaler, K., 1983. Rapid diffusion of the poloidal geomagnetic field through the weakly conducting mantle: a perturbation solution. Geophys. J. R. astr. Soc. 75, 77–100.

Bhattacharyya, A., 1995. An estimate of the radial gradient of the toroidal magnetic field at the top of the earth's core. Phys. Earth Planet. Inter. 90, 81–90.

Bronstein, I., Semendjajew, K., Musiol, G., Mühlig, H., 1997. Taschenbuch der Mathematik, 3. überarbeitete und erweiterte Auflage. Verlag Harri Deutsch, Thun, Franfurt am Main.

Buffett, B., 1992. Constraints on magnetic energy and mantle conductivity from the forced nutations of the earth. J. Geophys. Res. 97, 19581–19597.

Buffett, B., Mathews, P., Herring, T., 2002. Modeling of nutation and precession: Effect of electromagnetic coupling. J. Geophys. Res. 107, doi:10.1029/2000JB000056.

Celaya, M., Benton, E., 1991. Electromagnetic core-mantle coupling as a constraint on the toroidal field and conductivity in the mantle. Geophys. Astrophys. Fluid Dynamics 60, 376–378.

Ciarlet, P., Lions, J. (Eds.), 1990. Handbook of Numerical Analysis. Vol. I. Elsevier Science Publisher (North-Holland), Amsterdam, Ch. Finite Difference Methods for Linear Parabolic Equations.

Constable, S., Constable, C., 2004. Observing geomagnetic induction in magnetic satellite measurements and associated implications for mantle conductivity. Geochem. Geophys. Geosys 5, doi:10.1029/2003GC000634.

Dubrovinsky, L., Dubrovinskaia, N., Langhorst, F., Dobson, D., Ruble, D., Geßmann, C., Abrikosov, I., Johansson, B., Baykov, V., Vitos, L., Le Bihan, T., Crichton, W., Dmitriev, V., Weber, H.-P., 2003. Iron-silica interaction at extreme conditions and the electrically conducting layer at the base of earth's mantle. Nature 422, 58–61.

Greiner-Mai, H., 1986. Theoretische Betrachtungen zum Verhalten des Magnetfeldes in einem sphärischen Erdmodell. Astron. Nachr. 307, 201–208.

Greiner-Mai, H., 1987. The influence of the electromagnetic core-mantle coupling torques on earth's rotation. Astron. Nachr. 308, 217–226.

Greiner-Mai, H., 1993. Decade variations of the earth's rotation and geomagnetic core-mantle coupling. J. Geomag. Geoelectr. 45, 1333–1345.

Greiner-Mai, H., Ballani, L., Stromeyer, D., 2004. The poloidal geomagnetic field in a differentially rotating upper core layer. Geophys. J. Int. 158, 864–873.

Greiner-Mai, H., Hagedoorn, J., Ballani, L., Wardinski, I., Stromeyer, D., Hengst, R., 2007. Axial poloidal electromagnetic core-mantle coupling torque: A re-examination for different conductivity and satellite supported geomagnetic field models. Stud. Geophys. Geod. 51, 491–513.

Hagedoorn, J., Geiner-Mai, H., 2008. Core-Mantle Coupling - Part I: Electromagnetic coupling torques. Sci. Techn. Rep. GFZ Potsdam, STR 08/06 http://bib.gfz-potsdam.de/pub/str0806/0806.pdf.

Holme, R., 1998a. Electromagnetic core-mantle coupling – I. Explaining decadal changes in the length of day. Geophys. J. Int. 132, 167–180.

Holme, R., 1998b. Electromagnetic core-mantle coupling II: Probing deep mantle conductivity. In: Gurins, M., Wysession, M., Knittle, E., Buffet, B. (Eds.), The Core-Mantle Boundary Region. Vol. 28 of Geodynamics. AGU, pp. 139–151.

Jacobs, J. (Ed.), 1987. Geomagnetism. Vol. 2. Academic Press, London.

Jault, D., LeMouël, J.-L., 1991. Exchange of angular momentum between core and mantle. J. Geomag. Geoelectr. 43, 111–129.

Krause, F., Rädler, K.-H., 1980. Mean-Field Magnetohydrodynamics and Dynamo Theory. Akademie-Verlag, Berlin.

Kuvshinov, A., Olsen, N., 2006. A global model of mantle conductivity derived from 5 years of CHAMP, Ørsted, and SAC-C magnetic data. Geophys. Res. Lett. 33, doi:10.1029/2006GL027083.

Levy, E., Pearce, S., 1991. Steady state toroidal magnetic field at earth's core-mantle boundary. J. Geophys. Res. 96, 3935–3942.

Lin, J.-F., Watson, H., Vankó, G., Alp, E., Prakapenka, V., Dera, P., Struzhkin, V., Kubo, A., Zhao, J., McCammon, C., Evans, W., 2008. Intermediate-spin ferreous iron in lowermost mantle post-perovskite and perovskite. Nature geoscience 1, 688–691.

Love, J., Bloxham, J., 1994. Electromagnetic coupling and the toroidal magnetic field at the core-mantle boundary. Geophys. J. Int. 117, 235–256.

Nagao, H., Iyemori, T., Higuchi, T., Araki, T., 2003. Lower mantle conductivity anomalies estimated from geomagnetic jerks. J. Geophys. Res. 108, doi:10.1029/2002JB001786.

Olsen, N., 1998. The electrical conductivity of the mantle beneath Europe derived from c-response from 3 to 720 hr. Geophys. J. Int. 133, 298–308.

Ono, S., Oganov, A., Koyoma, T., Shimizu, H., 2006. Stability and compressibility of the high-pressure phases of Al_2O_3 up to 200 GPa: Implications for the electrical conductivity of the base of the lower mantle. Earth Planet. Sci. Lett. 246, 326–335.

Otha, K., Onoda, S., Hirose, K. Sinmyo, R., Shimizu, K., Sta, N., Ohishi, Y., Yasuhara, A., 2008. The electrical conductivity of post-perovskite in Earth's D'' layer. Science 320, 89–91.

Press, W., Teukolsky, S., Vetterling, W., Flannery, B., 1992. Numerical Recipes in Fortran. The Art of Scientific Computing. Cambridge University Press, Cambridge.

Pěč, K., Martinec, Z., 1988. Gravitational potential inside 3-D inhomogeneous Earth: a boundary-value problem for the Poisson equation. Studia geoph. et geod. 32, 32–46.

Roberts, P., 1972. Electromagnetic core-mantle coupling. J. Geomag. Geoelectr. 24, 231–259.

Rochester, M., 1960. Geomagnetic westward drift and irregularities in the Earth's rotation. Phil. Trans. R. Soc. Lond. A A 252, 531–555.

Rochester, M., 1962. Geomagnetic core-mantle coupling. J. Geophys. Res. 67, 4833–4836.

Stackhouse, S., 2008. The spin deep within. Nature geoscience 1, 648–650.

Stewart, D., Busse, F., Whaler, K., Gubbins, D., 1995. Geomagnetism, earth rotation and the electrical conductivity of the lower mantle. Phys. Earth Planet. Inter. 92, 199–214.

Stix, M., Roberts, P., 1984. Time-dependent electromagnetic core-mantle coupling. Phys. Earth Planet. Inter. 36, 49–60.

Varshalovich, D., Moskalev, A., Khersonskii, V., 1989. Quantum Theory of Angular Momentum. World Scientific, Singapore.

Velímský, J., Martinec, Z., Everett, M., 2006. Electrical conductivity in the earth's mantle inferred from CHAMP satellite measurements – I. Data processing and 1-D inversion. Geophys. J. Int. 166, 529–542.

Wardinski, I., 2005. Core surface flow models from decadal and subdecadal secular variation of the main geomagnetic field. Sci. Techn. Rep. GFZ Potsdam, STR 05/07 http://bib.gfz-potsdam.de/pub/str0507/0507.pdf.

Wardinski, I., Holme, R., 2006. A time-dependent model of the earth's mag-

netic field and its secular variation for the period 1980 – 2000. J. Geophys. Res. 111, doi:10.1029/2006JB004401.

Wardinski, I., Holme, R., Asari, S., Mandea, M., 2008. The 2003 geomagnetic jerk and its relation to the core surface flows. Earth Planet. Sci. Lett. 267, 468–481.

Xu, Y., McCammon, C., Poe, B., 1998a. The effect of alumina on the electrical conductivity of silicate peroviskite. Scinece 282, 922–924.

Xu, Y., Poe, B., Shankland, T., Rubie, D., 1998b. Electrical conductivity of Olevin, Wadsleyite, and Ringwoodite upper mantle conditions. Science 280, 1415–1417.

Xu, Y., Shankland, T., Poe, B., 2000. Laboratory-based electrical conductivity in the earth's mantel. J. Geophys. Res. 105, 27865–27875.

Zhang, F., Oganov, A., 2006. Valence state and spin transition of iron in Earth's mantle silicates. Earth Planet. Sci. Lett. 249, 436–443.

Zhang, K., Fearn, D., 1993. How strong is the invisible component of the magnetic field in the earth's core. Geophys. Res. Lett. 20, 2083–2086.